JCI The Journal of Clinical Investigation

Tumor fibroblast–derived epiregulin promotes growth of colitis-associated neoplasms through ERK

Clemens Neufert, Christoph Becker, Özlem Türeci, Maximilian J. Waldner, Ingo Backert, Katharina Floh, Imke Atreya, Moritz Leppkes, Andre Jefremow, Michael Vieth, Regine Schneider-Stock, Patricia Klinger, Florian R. Greten, David W. Threadgill, Ugur Sahin, Markus F. Neurath

J Clin Invest. 2013;123(4):1428-1443. https://doi.org/10.1172/JCI63748.

Research Article **Oncology**

Molecular mechanisms specific to colitis-associated cancers have been poorly characterized. Using comparative whole-genome expression profiling, we observed differential expression of epiregulin (EREG) in mouse models of colitis-associated, but not sporadic, colorectal cancer. Similarly, EREG expression was significantly upregulated in cohorts of patients with colitis-associated cancer. Furthermore, tumor-associated fibroblasts were identified as a major source of EREG in colitis-associated neoplasms. Functional studies showed that Ereg-deficient mice, although more prone to colitis, were strongly protected from colitis-associated tumors. Serial endoscopic studies revealed that EREG promoted tumor growth rather than initiation. Additionally, we demonstrated that fibroblast-derived EREG requires ERK activation to induce proliferation of intestinal epithelial cells (IEC) and tumor development in vivo. To demonstrate the functional relevance of EREG-producing tumor-associated fibroblasts, we developed a novel system for adoptive transfer of these cells via mini-endoscopic local injection. It was found that transfer of EREG-producing, but not Ereg-deficient, fibroblasts from tumors significantly augmented growth of colitis-associated neoplasms in vivo. In conclusion, our data indicate that EREG and tumor-associated fibroblasts play a crucial role in controlling tumor growth in colitis-associated neoplasms.

Tumor fibroblast–derived epiregulin promotes growth of colitis-associated neoplasms through ERK

Clemens Neufert,[1] Christoph Becker,[1] Özlem Türeci,[2] Maximilian J. Waldner,[1] Ingo Backert,[1] Katharina Floh,[1] Imke Atreya,[1] Moritz Leppkes,[1] Andre Jefremow,[1] Michael Vieth,[3] Regine Schneider-Stock,[4] Patricia Klinger,[4] Florian R. Greten,[5] David W. Threadgill,[6] Ugur Sahin,[2] and Markus F. Neurath[1]

[1]Medical Clinic 1, Friedrich-Alexander-Universität Erlangen-Nürnberg, Erlangen, Germany. [2]Institute for Translational Oncology (TRON), Universitätsmedizin der Johannes Gutenberg-Universität, Mainz, Germany. [3]Institute of Pathology, Klinikum Bayreuth, Bayreuth, Germany. [4]Institute of Pathology, Friedrich-Alexander-Universität Erlangen-Nürnberg, Erlangen, Germany. [5]Institute of Molecular Immunology, Klinikum Rechts der Isar, TU München, München, Germany. [6]Department of Genetics, North Carolina State University, Raleigh, North Carolina, USA.

Molecular mechanisms specific to colitis-associated cancers have been poorly characterized. Using comparative whole-genome expression profiling, we observed differential expression of epiregulin (EREG) in mouse models of colitis-associated, but not sporadic, colorectal cancer. Similarly, EREG expression was significantly upregulated in cohorts of patients with colitis-associated cancer. Furthermore, tumor-associated fibroblasts were identified as a major source of EREG in colitis-associated neoplasms. Functional studies showed that *Ereg*-deficient mice, although more prone to colitis, were strongly protected from colitis-associated tumors. Serial endoscopic studies revealed that EREG promoted tumor growth rather than initiation. Additionally, we demonstrated that fibroblast-derived EREG requires ERK activation to induce proliferation of intestinal epithelial cells (IEC) and tumor development in vivo. To demonstrate the functional relevance of EREG-producing tumor-associated fibroblasts, we developed a novel system for adoptive transfer of these cells via mini-endoscopic local injection. It was found that transfer of EREG-producing, but not *Ereg*-deficient, fibroblasts from tumors significantly augmented growth of colitis-associated neoplasms in vivo. In conclusion, our data indicate that EREG and tumor-associated fibroblasts play a crucial role in controlling tumor growth in colitis-associated neoplasms.

Introduction

Inflammatory bowel disease (IBD) is a present health problem believed to have a complex genetic and environmental etiology that can severely compromise the life quality of affected individuals of all ages. IBD involves an overactive immune response in genetically predisposed individuals driven by the bacterial flora (1–3). Aside from the symptomatic disease burden caused by relapsing intestinal inflammation, IBD patients are threatened by long-term complications including increased susceptibility to colorectal cancer (CRC) development. The elevated risk for colitis-associated cancer (CAC) is well documented for ulcerative colitis (UC) (4), and more recent studies provided evidence of an increased intestinal cancer development in individuals with Crohn's disease (CD) (5). Notably, the risk for CAC in IBD patients appears to be influenced by the inflammatory activity as well as the extent of colitis and duration of the disease. In fact, the severity of inflammation is a key risk factor for progression to colorectal neoplasia in UC (6). Even though the molecular mechanisms that explain how chronic inflammatory states contribute to the development of CAC are not fully understood, experimental models of colitis-associated tumorigenesis have suggested that chronic inflammation can facilitate tumor initiation and progression. In particular, it has been suggested that increased levels of reactive oxygen or nitrogen species may elevate the risk for mutations in intestinal epithelial cells (IEC) of the colon (7).

In humans, CACs share several characteristics with sporadic CRCs, which represent the most frequent group within the heterogeneous variety of CRCs. CAC and sporadic CRC also differ strikingly in numerous features (6). In sporadic CRC, healthy epithelium can typically turn into CRC in the adenoma-carcinoma sequence spanning several years. In contrast, CAC precursor lesions are often flat and multifocal, and such lesions may grow more rapidly.

Experimental data on molecular mechanisms that can modulate growth of CAC and sporadic CRC are increasing (8, 9). Numerous variables seem to be involved in influencing the development of intestinal neoplasms including the bacterial flora (10, 11). In addition, there are striking differences along the GI tract itself with respect to the cellular composition and the structure of the intestinal wall. Different regional susceptibilities for intestinal tumors are well known, but not sufficiently understood.

To improve translational relevance, our study focused on a direct comparison between experimental CAC and experimental sporadic CRC originating from the same rectosigmoid region of the lower GI tract that is the most frequent location for CAC and sporadic CRC in humans.

The molecular basis for characteristics specific to CAC as compared with sporadic CRC has not previously been clarified, although mechanisms such as different order of mutations in the multistep process of colon carcinogenesis have been hypothesized in humans (6). For the differential molecular analysis of CAC and sporadic CRC, we performed comparative whole-genome expression profiling between CAC and sporadic CRC in experimental

Conflict of interest: The authors have declared that no conflict of interest exists.
Citation for this article: *J Clin Invest.* 2013;123(4):1428–1443. doi:10.1172/JCI63748.

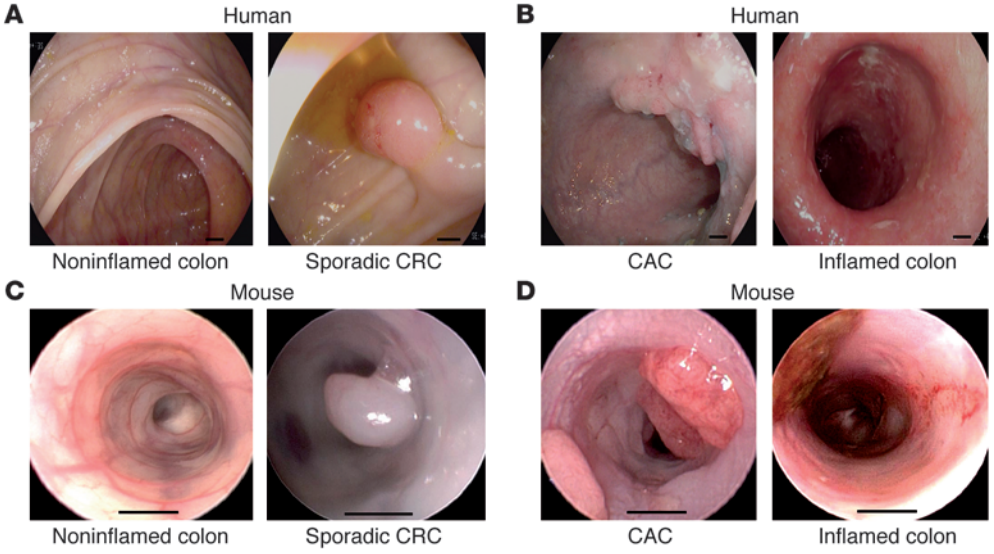

Figure 1
Growth features of sporadic and colitis-associated tumors. (**A**) Endoscopic images of patients without IBD. The left panel shows noninflamed colonic mucosal the right panel demonstrates a polypoid precursor lesion of a sporadic CRC with HGD, as confirmed by histopathological analysis. (**B**) Endoscopic pictures of patients suffering from UC. The right image demonstrates moderate intestinal inflammation (Mayo score 2); the left image displays a flat-appearing CAC, as confirmed by histopathological analysis. All images were acquired from the distal sigmoid colon, as documented by the colonoscopist. (**C** and **D**) Pictures from corresponding mouse models: noninflamed colon (**C**, left image), sporadic colorectal tumors in the *Apc*$^{min/+}$ model (**C**, right image), intestinal inflammation in the DSS model of colitis (**D**, right image), and colitis-associated neoplasms in the AOM/DSS model (**D**, left image). Scale bars: 2 mm.

mouse models and evaluated the potential role of differentially expressed candidate genes. Strikingly, functional studies including experiments with gene-deficient mice identified epiregulin (EREG) as a predominant regulatory factor for growth of CAC.

Results

Identification of EREG by whole-genome expression profiling in mouse models of CAC and sporadic CRC. To uncover molecules specifically involved in the pathogenesis of CAC, we studied tumorigenesis in experimental models of CAC and sporadic CRC that mimic key characteristics of human CRC (12–14). Whereas tumors in the *Apc*$^{min/+}$ model (where *Apc* indicates adenomatous polyposis coli) of sporadic CRC typically exhibit exophytic, pedunculated polyps, flat and multifocal tumors are characteristically observed in the azoxymethane/dextran sodium sulfate (AOM/DSS) model of CAC by endoscopy (Figure 1). To identify molecular mechanisms giving rise to such different growth patterns, we profiled gene expression in both models using high-density microarray analysis (HDMA). Tumor growth was monitored by repetitive mini-colonoscopy, and tissue was harvested when tumors reached a size covering between one-fourth and up to one-half of the colonic circumference, i.e., representing an endoscopic size score of 4 (15).

The cellular and molecular microenvironment of the intestinal wall has marked regional differences along the gastrointestinal (GI) tract; all tumors, including those from the *Apc*$^{min/+}$ model, were obtained from the distal part of the colon. To minimize stage-related differences in transcriptional profiles, all tumors were of the same size. Finally, to reduce the influence of different cellular compositions within the colonic wall, we used purified IEC from the distal colon as a control.

Whole-genome expression screening was performed with Affymetrix-GeneChips after purification of total RNA from tumors and respective control IEC. Hierarchical clustering as visualized by heat map analysis revealed groups of genes with similar expression patterns (Figure 2A). Expression profiles were then subjected to group-wise comparison, and advanced significance analysis between the tumors from both models revealed 924 probe sets (603 down, 321 up) with significance criteria of $P < 0.05$ after the Benjamini-Hochberg correction and at least a 2-fold change. The distribution of genes was visualized with a volcano plot (Figure 2B). The 25 genes with the greatest up or down differential expression showed a fold change (FC) ranging from 6 to 40 (Figure 2C). Among the genes with higher expression in the CAC model were several immune response–related genes such as *IgI-V1*, *IgkC*, or *Arg1*, which might be induced by immune cell infiltration. In addition, genes that have been related to tumor progression such as *Malat1* and *Klf5* were elevated in CAC. Among probe sets showing lower expression in the CAC model were several genes related to cell structure organization such as *Pfn2*, *Actn1*, and *Mark1*. Next, we performed Gene Ontology (GO) Enrichment Analysis using the list of differentially expressed upregulated genes, which identified GO terms such as cell proliferation, response to wounding, inflammatory response, and EGF binding in the CAC model compared with the sporadic CRC model (Figure 2D). In contrast, GO categories such as WNT receptor signaling pathway or TGF-β receptor signaling were not significantly enriched suggesting that no major differences exist in these pathways between the 2 models.

To further investigate differences, we performed significance analysis between the microarrays from the CAC model and control epithelia as well as the sporadic CRC model and control epithelia. This analysis revealed a high number of probe sets with differential expression ($P < 0.05$; FC > 2) (Figure 2E and Supplemental Table 1; supplemental material available online with this article; doi:10.1172/JCI63748DS1). By comparing these gene lists, we found overlapping gene expression patterns, as shown by Venn diagrams, and identified 387 probe sets that were exclusively upregulated in CAC but not in sporadic CRC (Figure 2F). We further refined our analysis by comparing the lists of probe sets "differentially upregulated in CAC model only" with the gene list "upregulated in CAC model versus sporadic CRC model" (Figure 2, B, E, and F). We obtained another list of genes, in which EREG, a member of the EGF family, ranked at position 3 of the most upregulated genes specific to CAC (Table 1). Of note, EREG was also identified on the list of top induced

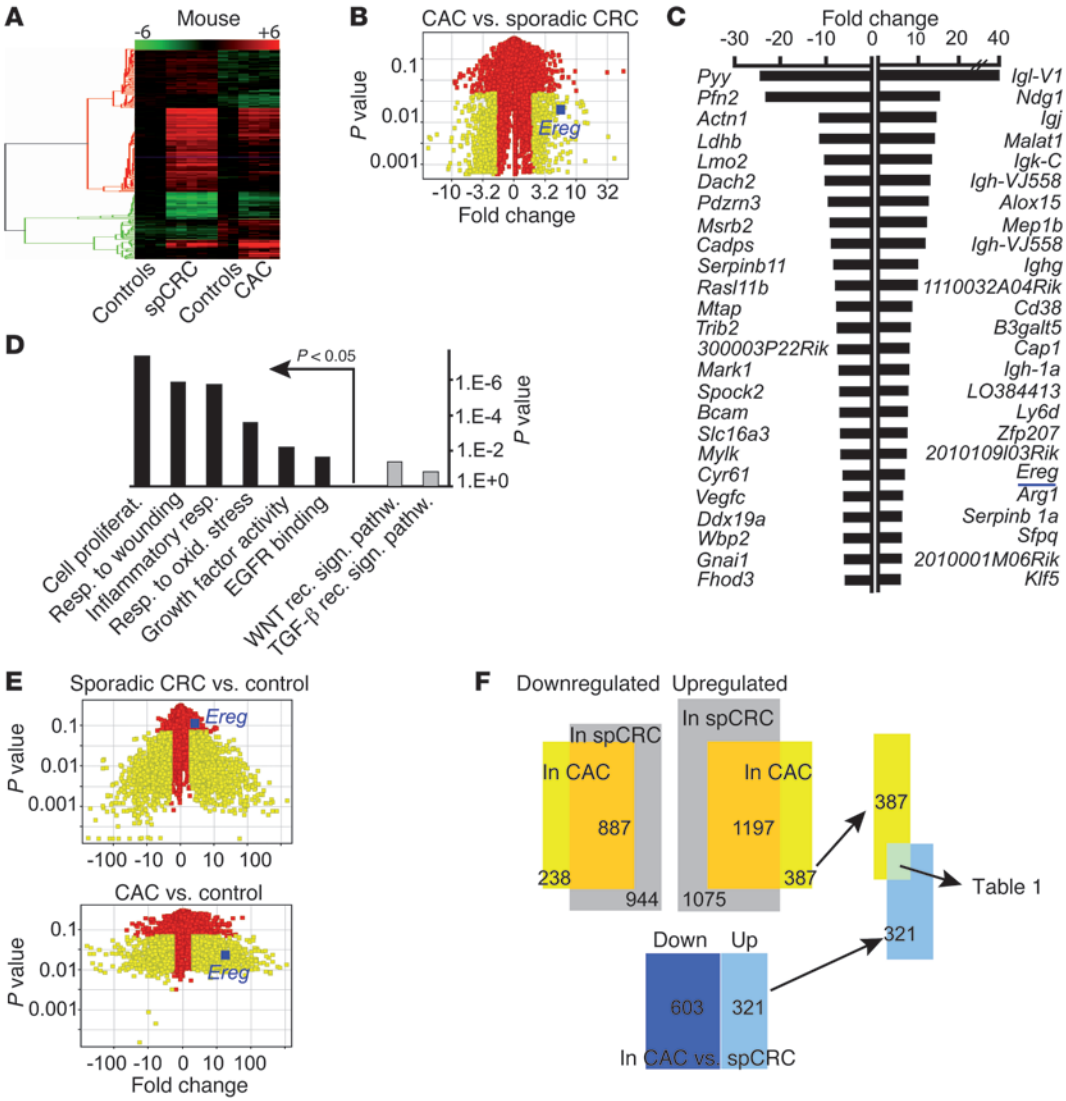

Figure 2

Differential gene expression studies in mouse models of sporadic and colitis-associated tumors identify EREG as a potential target. (**A**) Expression patterns from experimental models of CAC, sporadic CRC, and control epithelia were groupwise compared as described in Methods. (**B**) Distribution of transcripts from differential expression analysis (CAC vs. sporadic CRC) are displayed in a volcano plot (transcripts with $P < 0.05$ and FC > 2 in yellow). (**C**) The 25 significantly expressed genes with highest up- or downregulation are derived from differential expression analysis between CAC and sporadic CRC. (**D**) GO enrichment analysis was performed, as described in Methods. The displayed GO terms are derived from the genes that were differentially expressed with upregulation in the CAC model. Proliferat, proliferation; resp, response; oxid, oxidative; sign, signaling; rec, receptor; pathw, pathway. (**E**) Distribution of probe sets from differential expression analysis (CAC vs. control, sporadic CRC vs. control) are shown in volcano plots as indicated (transcripts with $P < 0.05$ and FC > 2 in yellow). (**F**) Gene lists from various differential expression analyses were compared with each other as visualized by Venn diagrams (blue, CAC vs. sporadic CRC; bright yellow, CAC vs. control; gray, sporadic CRC vs. control). The numbers of probe sets per group are displayed.

probe sets when a direct comparison between both tumor entities was performed (Figure 2C). Thus, EREG was differentially expressed between CAC and controls, CAC and sporadic CRC, but not sporadic CRC and controls (Figure 2, B and E). Surprisingly, other EGF-like ligands were not differentially expressed in the comparative analysis between the 2 models (Supplemental Figure 1), suggesting selective differential regulation of the EREG gene. Subsequent validation experiments using a larger panel of mouse tumors and control tissue by quantitative PCR (qPCR) confirmed the observations from HDMA.

Augmented EREG expression in UC patients with colitis-associated neoplasms. To investigate the potential relevance of EREG for human CRC, we next studied tissue from different stages of tumor development including sporadic and colitis-associated high grade dysplasias (HGDS) and sporadic CRC as well as CAC (Figure 3, A and B). Strikingly, the expression of EREG, as assessed by immunohistochemistry, was highly significantly elevated in colitis-associated dysplasias and carcinoma as compared with colonic tissue from control patients ($P < 0.01$). In contrast, the expression of EREG in specimens from sporadic

Table 1
Gene list from differential gene expression analysis in experimental colon cancer models

Gene symbol	CAC vs. control (FC)	CAC vs. sporadic CRC (FC)
Igl-V1	43.0	32.3
Ndg1	22.9	15.1
Ereg	16.6	6.4
Lgals2	11.1	3.2
Aldh1a3	6.4	3.7

The 5 most induced genes of the overlapping subgroup in Figure 2F.

tumor development was lower, although still elevated at the average level compared with normal colonic tissue. Of note, EREG expression appeared to be more heterogenous in sporadic as compared with colitis-associated neoplasms. Consistently, quantitative analysis of EREG expressing cells revealed a significant increase in colitis-associated neoplasms (UC-associated HGDs and cancer) as compared with sporadic neoplasms (sporadic HGDs and cancer) (Figure 3C).

Additional differences between sporadic and UC-associated neoplasms were noted with regard to the cellular source of EREG production. In particular, we detected that EREG expression in colitis-associated tumors was dominated by tumor stromal cells, whereas EREG expression in sporadic tumors was often found in patches of epithelial cells that showed basolateral EREG enrichment. Taken together, these findings highlighted the potential functional relevance of EREG in UC-associated tumor lesions in humans.

EREG deficiency impairs colitis-associated tumor growth. Since data using gene expression profiling and immunohistochemistry were consistent with a potential regulatory role of EREG in colitis-associated tumors, we next addressed the functional role of this growth factor in experimental tumorigenesis. In these studies, we took advantage of $Ereg^{-/-}$ mice and performed experiments using the AOM/DSS model of colitis-associated tumor growth. Strikingly and in marked contrast to previous studies on sporadic intestinal tumorigenesis in the $Apc^{min/+}$ small intestinal model (16), $Ereg^{-/-}$ mice were strongly protected from tumor develop-

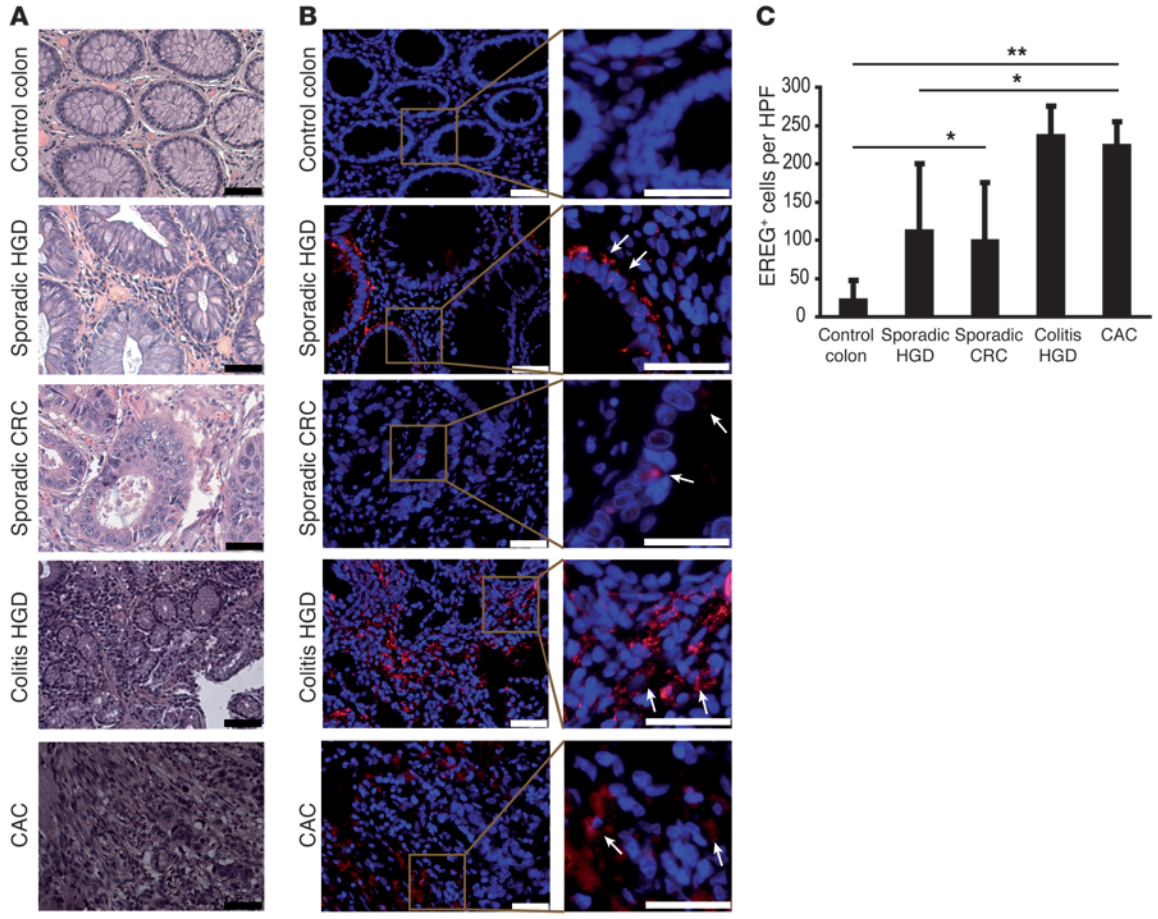

Figure 3
Human precursor lesions of colitis-associated tumors display significantly elevated EREG expression. (**A**) H&E stainings of paraffin-embedded tissue sections from colorectal tumors and control tissue, as indicated. Scale bars: 50 μm. (**B**) Immunostaining for human EREG in the same samples as in **A**. The analysis included 47 samples (non-IBD control group, $n = 7$; sporadic HGD, $n = 12$; sporadic CRC, $n = 11$; colitis-associated HGD, $n = 9$; CAC, $n = 8$). Scale bars: 50 μm. (**C**) For quantitative analyses, 4–5 representative high power fields (HPF) per sample were scored for the number of positive cells. Original magnification, ×40. Data are shown as mean values per group ± SD. Significant differences are indicated. $^*P < 0.05$; $^{**}P < 0.01$.

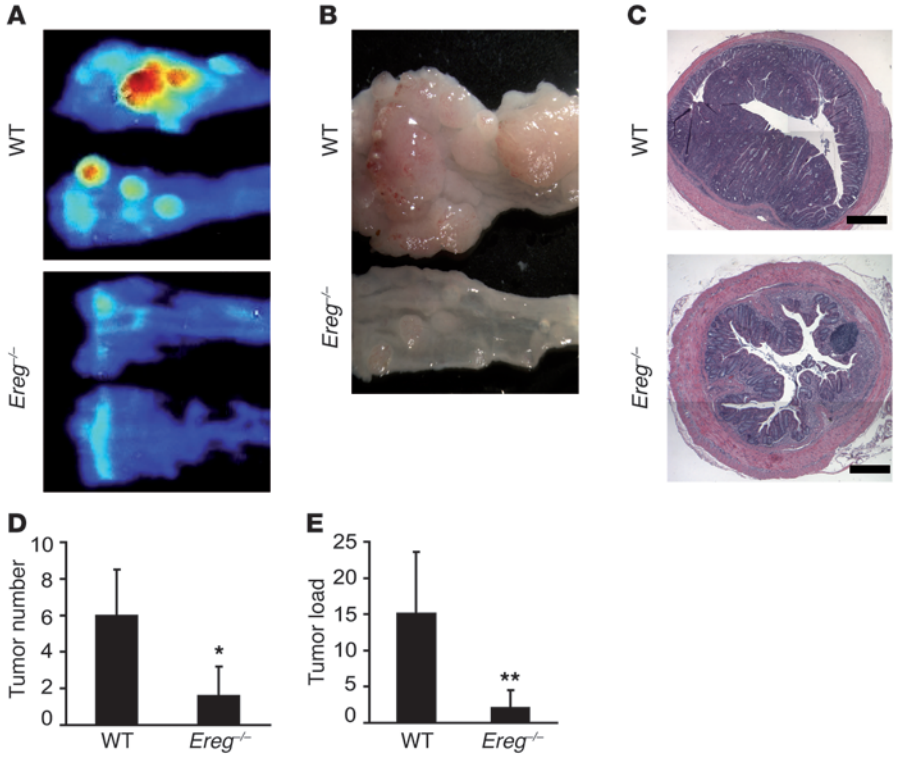

Figure 4
Colitis-associated tumorigenesis in *Ereg*-deficient mice. (**A**–**C**) Colitis-associated tumors were induced in WT controls and *Ereg*$^{-/-}$ mice by AOM and 3 cycles of DSS. Tumor development in the rectosigmoid was assessed by multispectral fluorescence imaging of integrin $\alpha_V\beta_3$, stereomicroscopic inspection, and histopathological analysis at day 80 as shown by representative pictures of each group. Scale bars: 400 μm. Both images in **C** are composites of multiple overlapping images to allow a broader field of view. (**D** and **E**) Total tumor numbers and average tumor load per mouse were quantified in WT controls and *Ereg*$^{-/-}$ mice. Data are shown as mean values ± SD of 8–10 mice per group, and similar results were obtained in 3 independent experiments. **P* < 0.05; ***P* < 0.01.

ment in the mouse AOM/DSS colonic model. This observation was verified by in vivo imaging of integrin $\alpha_V\beta_3$, macroscopic inspection, high-resolution endoscopy, and histopathological analysis of H&E-stained cross sections (Figure 4, A–E). In fact, endoscopic scoring demonstrated a significant difference in the tumor load between *Ereg*$^{-/-}$ mice and WT controls ($P < 0.01$). Of note, although we detected a difference in tumor numbers (Figure 4D), the striking difference in tumor load (Figure 4E) was particularly caused by significant differences in tumor sizes between WT and *Ereg*$^{-/-}$ mice (Figure 5). To analyze the kinetics of tumor development in both groups, we performed serial endoscopies in longitudinal studies directly addressing tumor growth over time. Whereas early neoplastic lesions were detected around days 15 to 20 in both groups, tumor load analysis showed an increasing difference between WT and *Ereg*$^{-/-}$ mice at later time points (Figure 5, A and B). In fact, endoscopic analyses suggested that tumor growth is inhibited in *Ereg*$^{-/-}$ mice at later time points, resulting in slower growth rates and a persistent majority of small tumors compared with the composition of tumor load in WT controls. In WT mice, almost one-fourth of all tumors were large (sizes 4 or 5) at day 80. In contrast, large tumors were not observed in *Ereg*$^{-/-}$ animals by day 80 and very small tumors (size 1) accounted for more than 50% of all tumors in *Ereg*$^{-/-}$ mice even at day 80 (Figure 5C). Thus, the strong reduction in tumor load over time in *Ereg*$^{-/-}$ mice is due to a reduction of large tumors, suggesting a key role of EREG in tumor growth promotion rather than initiation.

EREG regulates epithelial wound healing and promotes tumor growth. As previous studies demonstrated a direct link between inflammatory activity and tumor growth in experimental colitis-associated tumorigenesis (17, 18), we next addressed EREG expression during DSS-induced colonic inflammation. Consistent with previous findings showing a strong temporary increase in intestinal EREG levels in acute colitis (19), we noted repeated more than 10-fold upregulation of EREG expression during DSS cycles, mimicking flares of increased activity in IBD (Figure 6A). Interestingly, we observed a slight increase of average EREG expression over time, suggesting a marked and repeated EREG induction by flares in chronic intestinal inflammation. Although *Ereg*$^{-/-}$ mice were more susceptible to acute DSS colitis than WT controls (16), no significant differences in colonic inflammation between these mouse strains were found during chronic DSS colitis (Supplemental Figure 2). Thus, although EREG expression is induced by inflammation, this protein does not seem to importantly regulate activity of chronic intestinal inflammation.

To explore possible alternative functions of EREG, we performed studies on the role of this protein in epithelial wound healing. In initial studies, we used an in vitro assay for cell migration in which a mouse colonic epithelial cell line (CMT93) was grown to confluence before gaps of defined size were scratched into the cell layer. Subsequently, cells were cultured in the presence or absence of EREG followed by assessment of gap sizes. Strikingly, wound gap closure in the presence of EREG was significantly accelerated (about 50% of remaining gap size after 18 hours compared with untreated cells), suggesting a prominent role of EREG during reconstitution after epithelial injury (Figure 6, B and C). To study whether EREG also contributes to intestinal wound gap closure in vivo, we generated epithelial defects in the distal colon of *Ereg*$^{-/-}$ mice and control animals by use of the biopsy forceps in mini-endoscopy. Wound healing was monitored by serial endoscopy (20). Consistent with our data from in vitro experiments, intestinal wound healing was significantly delayed in *Ereg*$^{-/-}$ mice compared with controls, indicating a major regulatory function of EREG in epithelial wound healing in vivo (Figure 6,

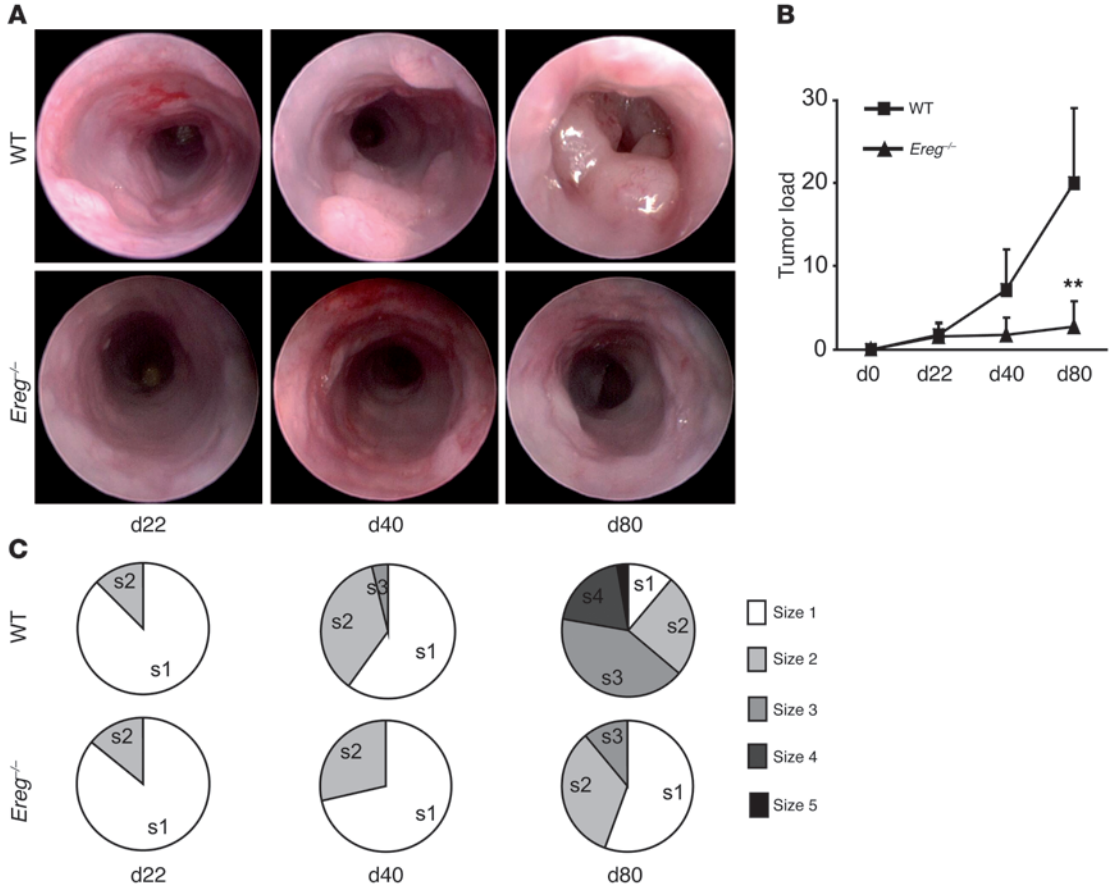

Figure 5

EREG promotes growth rather than initiation of colitis-associated tumors. (**A** and **B**) Serial analyses of AOM/DSS tumors was performed in controls and *Ereg*$^{-/-}$ mice by endoscopy, as indicated. Tumor load development over time is shown by representative endoscopic pictures and average tumor load progression analysis. (**C**) The relative contribution of different tumor sizes (s1 = small, s5 = very large) to the total tumor load in WT and *Ereg*$^{-/-}$ mice was determined. The serial analysis was performed with 5 mice per group and was repeated twice with similar results. Data are shown as mean values ± SD. $^{**}P < 0.01$.

D and E). Consistently, studies with heterozygous lacZ-*Ereg*-reporter mice demonstrated the accumulation of EREG-producing cells around the wound bed in response to in vivo wounding in the distal colon (Figure 6F).

To directly demonstrate effects of EREG on epithelial cell proliferation, full-thickness rectosigmoidal pieces were incubated with mock or recombinant EREG and stained for Ki67 (Figure 7, A and B). EREG treatment led to a significant increase of epithelial cell proliferation ($P < 0.05$). To test whether EREG could directly increase the number of IECs and promote growth of colon tumors, we applied recombinant EREG to CMT93 cells and early colon tumors in vivo. Interestingly, we observed a significant increase in epithelial cell numbers after incubation in the presence of EREG, providing further evidence for an increase in proliferation mediated by EREG ($P < 0.05$). Of note, the number of cells showed a dose-dependent increase in the presence of EREG at 48 hours compared with control cells (Figure 7C). We next injected EREG or other EGF-like ligands into WT mice during AOM/DSS treatment and performed endoscopic tumor screening at day 30 (Figure 7D). We chose animals with similar tumor load and performed local injections of EREG, EGF, amphiregulin (AREG), or equal volumes of PBS. The injections were applied during endoscopy using a flexible syringe device near the base of similar sized small tumors every 3–4 days. Tumor growth was monitored by endoscopy, and mice with EREG injections displayed a significantly accelerated increase in tumor load compared with mice that had obtained PBS injections ($P < 0.05$). In contrast, other EGFR ligands such as EGF and AREG were less potent and did not result in a significant increase of tumor load as compared with the PBS control group (Figure 7, E and F).

In summary, these observations suggest that colitis-associated EREG expression promote not only intestinal wound healing, but also tumor growth.

Identification of tumor-associated fibroblasts as the key cellular source of EREG in colitis-associated neoplasms. The cellular source of EREG has been assigned to epithelial and submucosal cells during acute inflammation (16). To identify the cellular source of EREG in the AOM/DSS model of CAC, we took advantage of the LacZ reporter gene knockin of *Ereg*-deficient mice and performed X-gal stainings in heterozygous animals. It was found that the majority of cells that stained positive for EREG in AOM/DSS tumors were stromal cells (Figure 8A). In addition, we detected some EREG-expressing epithelial cells. As fibroblasts display a frequent cell type in the tumor microenvironment that may produce regula-

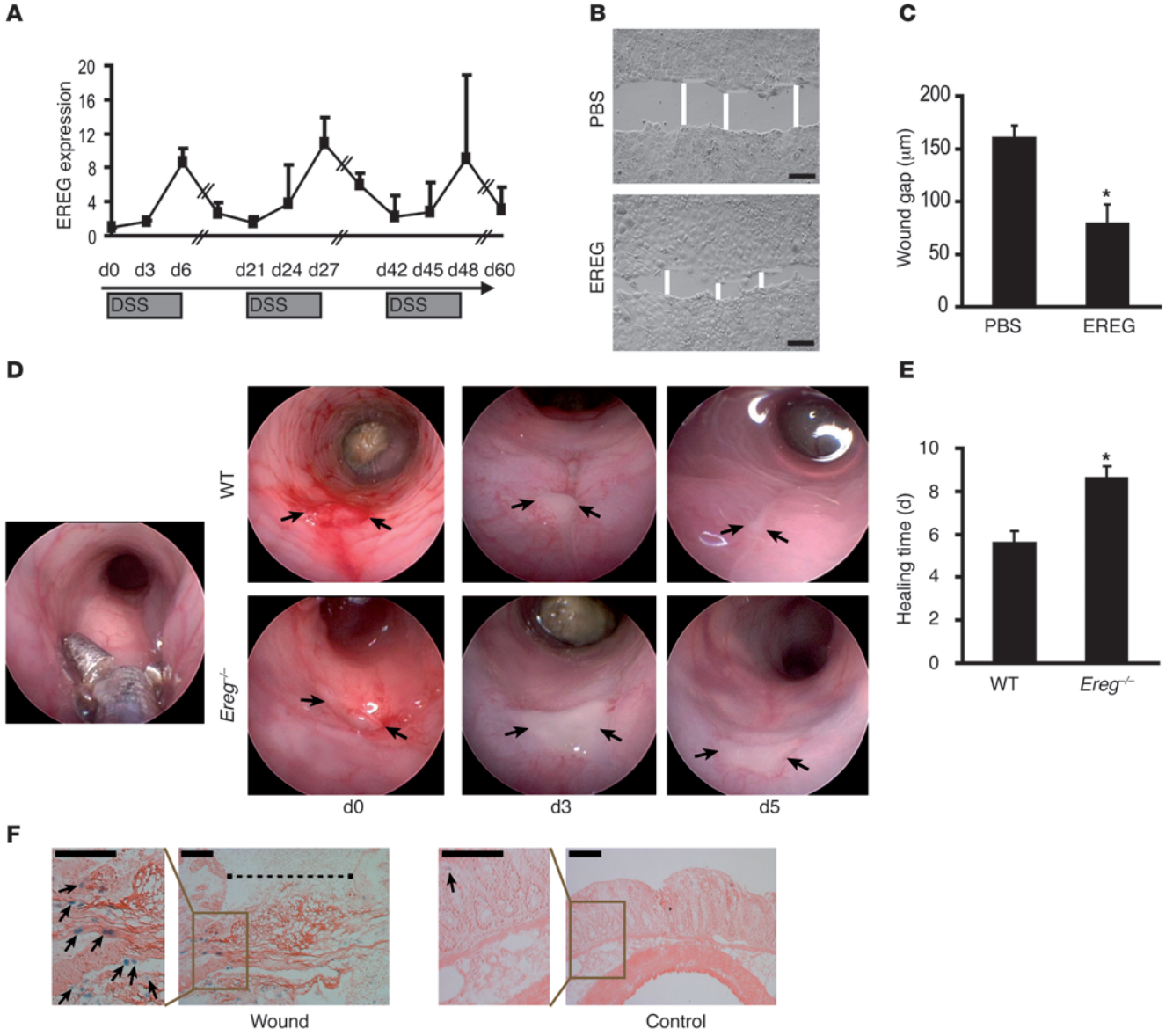

Figure 6

EREG facilitates intestinal wound healing in vitro and in vivo. (**A**) Experimental colitis was induced by 3 cycles of DSS. EREG expression was measured in the distal colon by qPCR. Data are mean values ± SD of 2–4 animals per data point. Similar results were obtained in 2 independent experiments. (**B** and **C**) Gaps were scratched into monolayers of IEC. PBS or EREG (100 ng/ml) was applied, and the wound gap closure was analyzed by microscopy after 18 hours. Representative images from 1 experiment out of 3 are shown. Scale bars: 100 μm. Data shown as mean values ± SD. **P* < 0.05. (**D** and **E**) In vivo wounding was performed by targeted biopsies in control (*n* = 4) and *Ereg*$^{-/-}$ (*n* = 4) mice. The mucosal healing was monitored by endoscopy every 1–2 days. Representative images are displayed from days 0, 3, and 5. The experiment was repeated twice with similar results. Arrows highlight the margins of the mucosal lesions. **P* < 0.05. (**F**) Cross sections of the in vivo wounded distal colon (d3, left panel) from EREG-reporter mice (*Ereg*$^{+/-}$) were analyzed by X-gal staining. The dotted line indicates the wound gap. Control tissue (right panel) was obtained from the unwounded distal colon of the same mouse. Numerous EREG-expressing cells (arrows) could be identified adjacent to the wound but not in control tissue. Scale bars: 100 μm.

tory molecules (21), we next addressed the possibility that cancer-associated fibroblasts are the major cellular source of EREG production in AOM/DSS tumors.

To test this hypothesis, we performed consecutive stainings of cross sections from AOM/DSS-tumors of heterozygous lacZ-*Ereg*-reporter mice by using both X-gal staining and confocal immunohistochemistry. Here. we could show that over two-thirds of all EREG-expressing cells and virtually all EREG-expressing stromal cells colocalized with fibroblast markers including vimentin (VIM) and fibroblast-specific protein-1 (FSP1, also known as S100A4) (Figure 8, A and B). A similar expression pattern could be demonstrated for PDGFR-β (Figure 8A). In addition, approximately 60% of EREG-expressing stromal cells could be colocalized with α-SMA (Figure 8A), indicating an activated myofibroblastic phenotype in a substantial

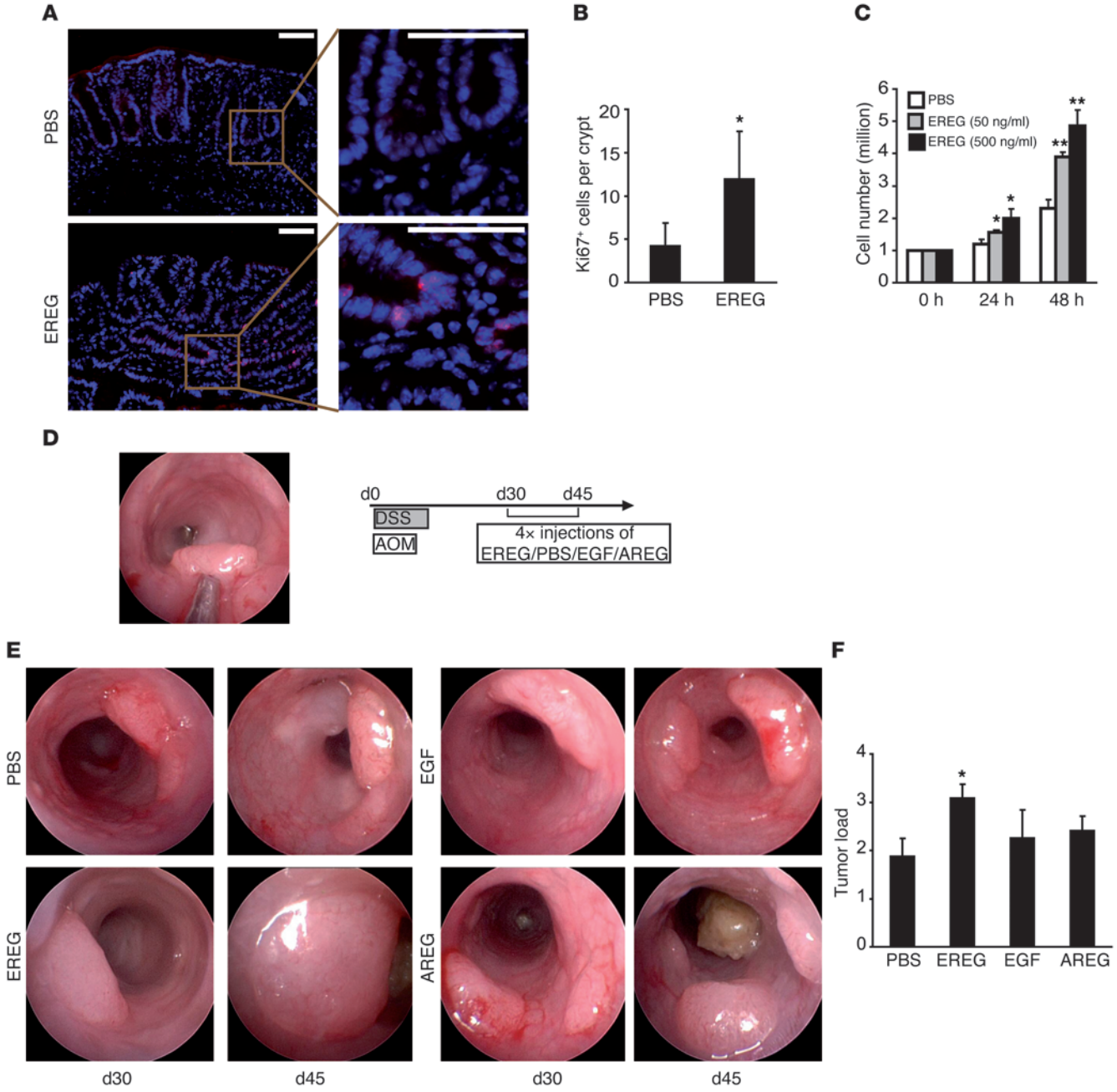

Figure 7

EREG directly increases proliferation in IECs and promotes colon tumor growth. (**A**) Full-thickness rectosigmoidal pieces were incubated with PBS or EREG (500 ng/ml) and analyzed by immunohistochemistry for Ki67. Representative images out of 3 experiments are shown. Scale bars: 100 μm. (**B**) Staining was quantified by counting of positive cells per crypt. *$P < 0.05$. (**C**) IEC were grown in 12-well plates with varying concentrations of EREG. Cell numbers were determined after 24 and 48 hours. The experiment was performed in duplicate and repeated 3 times with similar results. *$P < 0.05$; **$P < 0.01$. (**D**–**F**) Rectosigmoidal tumors were induced in WT animals by AOM and 1 cycle of DSS. Starting at day 30, repeated injections of PBS ($n = 5$), recombinant EREG ($n = 5$), EGF ($n = 3$), or AREG ($n = 3$) were performed in the base of small tumors 4 times in 10 days. The change in tumor load was assessed by endoscopy at day 45. Data from 1 out of 2 experiments are shown and represent mean values ± SD. *$P < 0.05$.

number of EREG-expressing cells in colitis-associated tumors. To verify whether tumor-associated fibroblasts represent also a major cellular source of EREG in CAC in humans, in an additional series of experiments, we stained samples from patients with UC-associated colorectal neoplasms with antibodies against fibroblast markers and EREG. In congruence with our observations from the mouse model of CAC, EREG-expressing stromal cells in human CAC demonstrated coexpression with the fibroblast marker VIM (Figure 8C), suggesting that EREG-producing tumor-associated fibroblasts are present in both murine and human colitis-associated neoplasms.

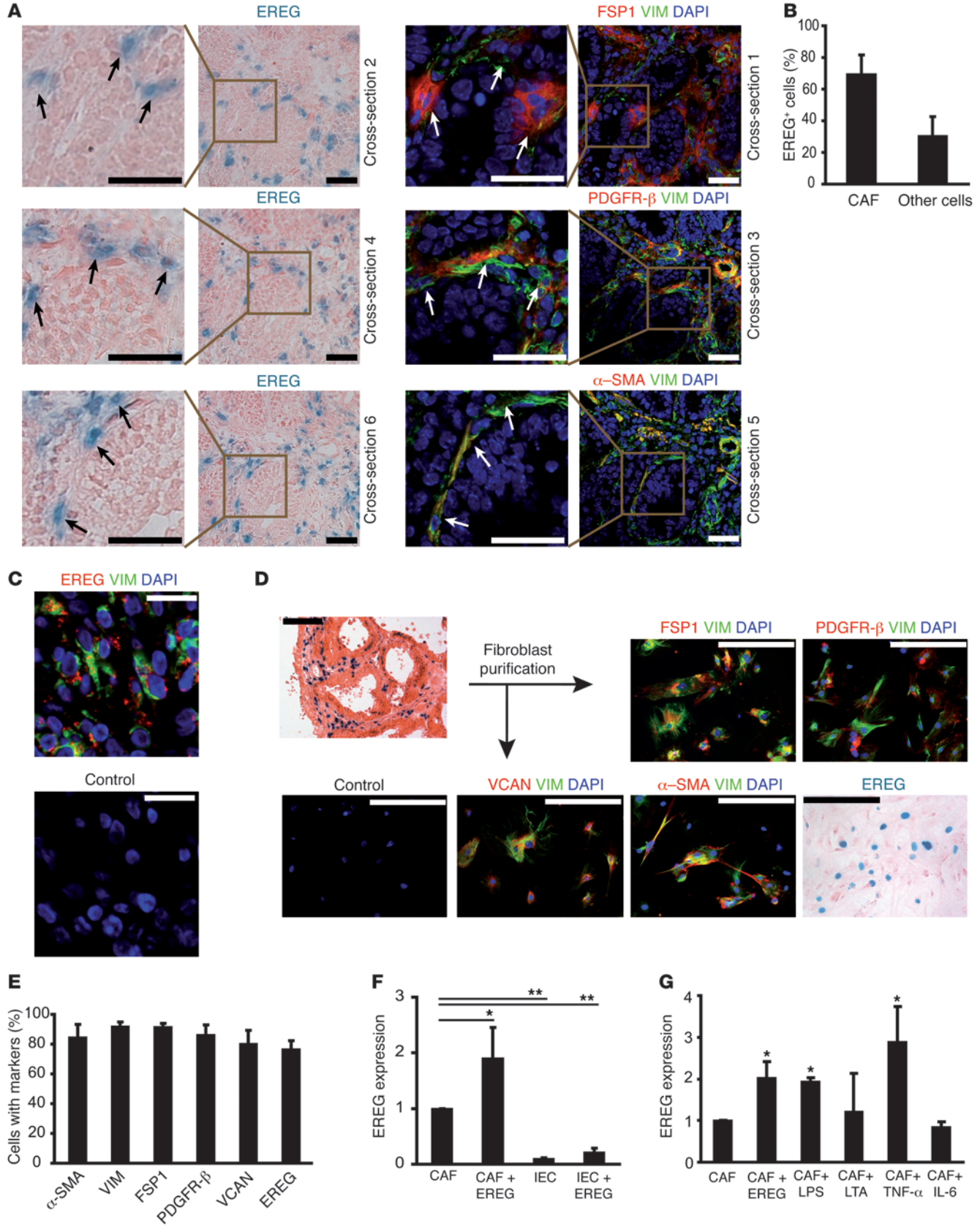
A
EREG
FSP1 VIM DAPI
Cross-section 2
Cross-section 1
EREG
PDGFR-β VIM DAPI
Cross-section 4
Cross-section 3
EREG
α–SMA VIM DAPI
Cross-section 6
Cross-section 5
B
EREG+ cells (%)
100
80
60
40
20
0
CAF
Other cells
C
EREG VIM DAPI
Control
D
Fibroblast purification
FSP1 VIM DAPI
PDGFR-β VIM DAPI
Control
VCAN VIM DAPI
α–SMA VIM DAPI
EREG
E
Cells with markers (%)
100
80
60
40
20
0
α-SMA
VIM
FSP1
PDGFR-β
VCAN
EREG
F
EREG expression
3
2
1
0
*
**
**
CAF
CAF + EREG
IEC
IEC + EREG
G
EREG expression
4
3
2
1
0
*
*
*
CAF
CAF + EREG
CAF+ LPS
CAF+ LTA
CAF+ TNF-α
CAF+ IL-6

Figure 8
Fibroblasts are the main producers of EREG in colitis-associated tumors. (**A**) Consecutive rectosigmoidal cross sections (nos. 1–6) of 4-μm thickness from AOM/DSS-tumors of lacZ-*Ereg*-reporter mice were stained with X-gal plus eosin (left panels) or with specific antibodies against fibroblast markers as indicated (right panels). Representative brightfield and confocal immunohistochemical images are shown. Arrows indicate double-positive cells in consecutive sections. Scale bars: 25 μm. (**B**) Tumor cells with positive X-gal staining were quantified for colocalization with markers VIM, FSP1, and PDGFR-β of cancer-associated fibroblasts (CAF). Data represent mean values ± SD from 5 tumors. (**C**) Human cross sections from a patient with UC and HGD were stained for EREG and VIM (left panel) or with an antibody control (right panel) and studied by confocal laser microscopy. Scale bars: 25 μm. (**D** and **E**) Fibroblasts were purified from AOM/DSS tumors of $Ereg^{+/-}$ mice as specified in Methods and grown in cell culture. At day 5, cells were analyzed for α-SMA, VIM, FSP1, PDGFR-β, and VCAN by immunocytochemistry as indicated. Additionally, EREG expression was determined by X-gal staining. Scale bars: 50 μm. (**F** and **G**) Fibroblasts from AOM/DSS tumors were isolated and cultured with PBS, EREG (100 ng/ml), LPS (1000 ng/ml), LTA (1000 ng/ml), TNF-α (100 ng/ml), or IL-6 (100 ng/ml) for 6 hours. EREG expression was measured by qPCR. Data represent mean values ± SD (n = 2–3 per group). Similar results were obtained in 2 independent experiments. $^*P < 0.05$; $^{**}P < 0.01$.

To further characterize EREG-producing cells in colitis-associated neoplasms, we next isolated fibroblasts from AOM/DSS tumors of heterozygous lacZ-*Ereg*-reporter mice. The purity of these fibroblast cultures was assessed by immunocytochemical analysis, which revealed a high number of cells expressing proteins related to tumor-associated fibroblasts including VIM (>90%), FSP1 (>90%), PDGFR-β (90%), versican (VCAN, also known as chondroitin sulfate proteoglycan 2 or NG2) (85%), and α-SMA (80%). Strikingly, EREG expression was seen in more than 75% of the cells in these fibroblast cultures, as demonstrated by X-gal stainings (Figure 8, D and E).

Whereas lacZ staining was useful to localize and count the number of EREG-expressing cells in murine cell culture, we took advantage of real-time qPCR to quantify the expression of EREG in tumor fibroblasts. Remarkably, these cells produced high amounts of EREG and a significant, more than 10-fold difference in EREG production was noted between tumor-associated fibroblasts and IEC (Figure 8F). Of note, the addition of recombinant EREG to tumor fibroblasts significantly increased EREG production, suggesting the presence of additional self-perpetuating autocrine and paracrine loops in these cells (Figure 8F).

In subsequent experiments, we aimed at the identification of signaling pathways inducing EREG expression in tumor-associated fibroblasts. It was found that tumor-associated fibroblasts produce high baseline levels of EREG, which could be further enhanced by in vitro stimulation with LPS or TNF-α (Figure 8G). As TNF-α and bacterial proteins such as LPS are thought to play a major role in IBDs (1, 22), these findings suggested that microbial products and proinflammatory molecules released during intestinal inflammation are important inducers of local EREG production by tumor-associated fibroblasts in colitis-associated neoplasms.

Adoptive transfer of EREG-producing tumor-associated fibroblasts promotes tumor growth in colitis-associated neoplasms in vivo. In subsequent studies, we analyzed whether tumor fibroblast–derived EREG may affect growth of IEC. Accordingly, mouse IEC (cell line CMT93) were grown in the presence of conditioned medium from AOM/DSS tumor fibroblasts purified from WT and $Ereg^{-/-}$ mice, respectively. Strikingly, the conditioned medium obtained from the WT tumor fibroblasts resulted in a significant increase in the epithelial cell number after 48 hours, whereas the conditioned medium from $Ereg^{-/-}$ cells did not induce significant changes in cell numbers (Figure 9A). These findings indicated that fibroblast-derived EREG favors proliferation of IEC.

In subsequent studies, we addressed the possibility that EREG derived from tumor fibroblasts augments growth of colitis-associated neoplasms in vivo. To further evaluate the in vivo relevance of fibroblast-derived EREG production for the growth of CAC in the AOM/DSS model, we intended to set up studies with adoptive transfer of tumor-derived fibroblasts. Accordingly, we developed an adoptive transfer system of fibroblasts via endoscopically guided local injections into small tumors (endoscopic tumor score 1). In a first set of experiments, we validated this injection technique and injected portions of 50 μl of a fibroblast suspension from heterozygous lacZ-*Ereg*-reporter mice (10^5 cells) into tumors of WT mice. At day 2 after injection, tumors were harvested and stained for X-gal to assess EREG expression. These studies demonstrated not only the presence of transferred fibroblasts surrounding the tumor tissue, but also showed EREG expression in transferred cells within the tumor stroma (Figure 9, B and C).

We next treated $Ereg^{-/-}$ mice with AOM and 1 cycle of DSS and performed endoscopic tumor screening at day 30 to ensure equal average tumor scores in all groups. We then injected $Ereg^{-/-}$ or WT fibroblasts from AOM/DSS-treated mice into small tumors of these $Ereg^{-/-}$ mice during endoscopy every 5 days. An additional group of WT mice did not receive tumor-associated fibroblasts and served as a control group. In consecutive studies, changes in tumor load were monitored endoscopically in all 3 groups of animals (Figure 9, D–F). AOM/DSS-treated $Ereg^{-/-}$ mice repetitively injected with $Ereg^{-/-}$ fibroblasts showed significantly slower tumor growth as compared with AOM/DSS treated $Ereg^{+/+}$ (WT) mice without fibroblast injections ($P < 0.05$). However, *Ereg*-deficient mice given WT fibroblasts showed significantly augmented tumor growth as compared with *Ereg*-deficient mice given *Ereg*-deficient fibroblasts (Figure 9, E and F), suggesting that EREG from tumor-associated fibroblasts induces tumor growth in vivo. Furthermore, $Ereg^{-/-}$ animals repetitively treated with WT tumor fibroblasts showed no significant differences compared with AOM/DSS-treated WT control mice, suggesting that adoptive transfer of EREG-producing but not EREG-deficient tumor-associated fibroblasts is sufficient to abrogate the differences in tumor growth between WT and *Ereg*-deficient mice. In summary, these observations indicate that colitis-associated EREG expression by tumor fibroblasts can promote tumor growth in the AOM/DSS model in vivo.

A key role of ERK in EREG-mediated regulation of cell proliferation. EREG belongs to the EGF-like family of growth factors that can signal through of ERBB receptors, which can activate several pathways potentially involved in tumor growth such as ERK (also known as ERK1/2, MAPK3/1, or p44/p42-MAPK), p38-MAPK, and STAT3 pathways (23). Thus, we tested a number of downstream targets potentially involved in EREG signaling in our experimental model of CAC. Our data showed that EREG causes a pronounced activation of ERK in IEC in vitro (Figure 10A). In contrast, other major pathways related to tumor development including p38-MAPK and STAT3 showed little or no changes upon stimulation with EREG (data not shown).

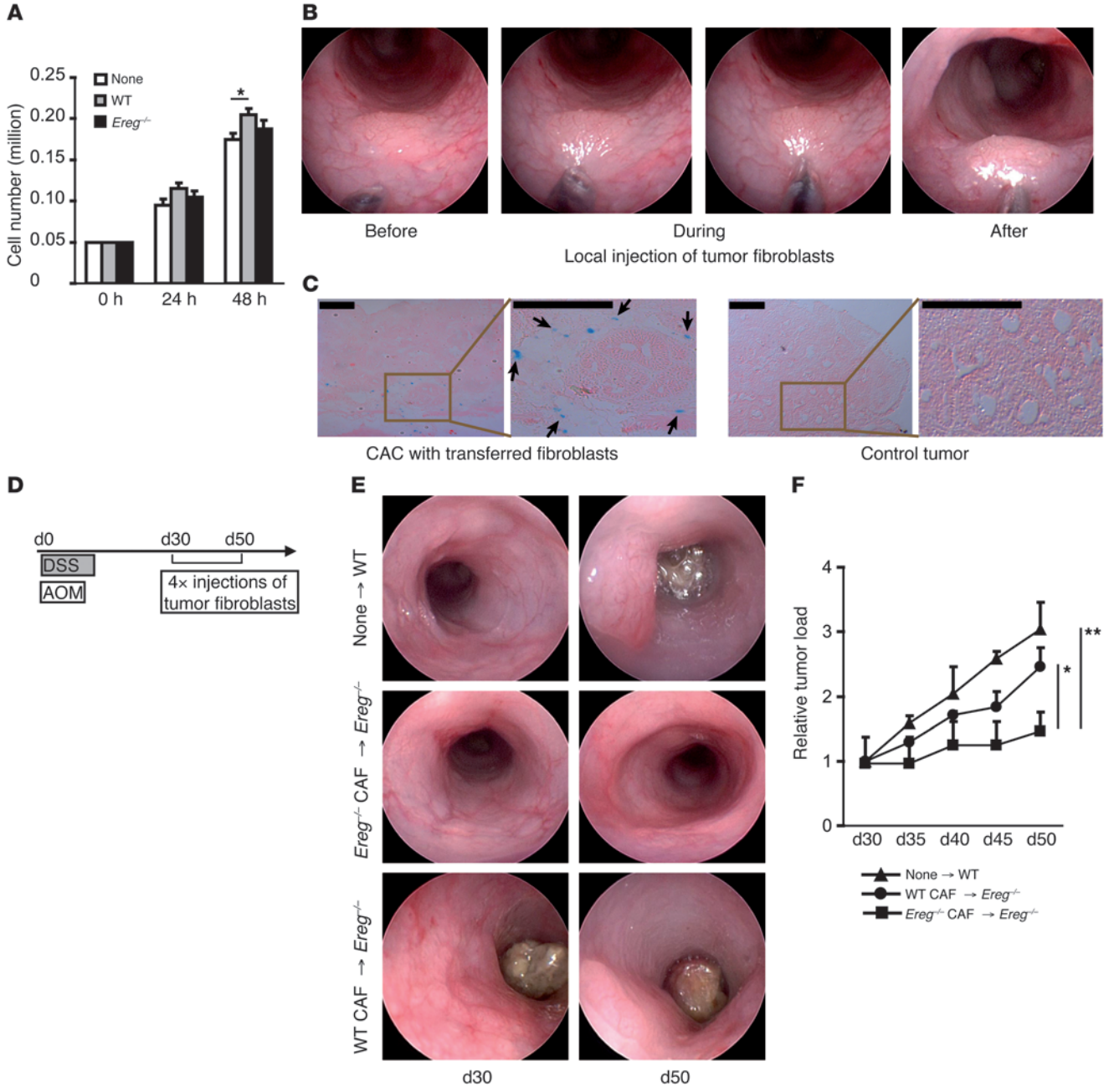

Figure 9

Adoptive transfer model: fibroblast-derived EREG promotes the growth of colitis-associated tumors. (**A**) IEC were grown in 48-well plates with conditioned medium from *Ereg*$^{-/-}$ or WT tumor fibroblasts, and cell numbers were determined after 24 and 48 hours. The experiment was performed in triplicate and repeated twice with similar results. **P* < 0.05. Data represent mean values ± SD. (**B** and **C**) Fibroblasts from AOM/DSS tumors of heterozygous lacZ-*Ereg*-reporter mice were endoscopically injected into a tumor of a WT mouse. At day 2 after injection, the tumor was harvested, and cross sections were stained for X-gal. EREG-expressing fibroblasts were identified in the tumor stroma upon cell transfer (arrows). Scale bars: 100 μm. (**D**–**F**) *Ereg*$^{-/-}$ and WT mice were treated with AOM and 1 cycle of DSS. Starting at day 30, repeated injections (4 times in 15 days) of tumor fibroblasts from *Ereg*$^{-/-}$ or WT animals were performed into the base of small tumors of *Ereg*$^{-/-}$ mice (*n*= 3 per group). The change in tumor load was endoscopically monitored until day 50. Data are from 1 out of 2 independent experiments with similar results and represent mean values ± SD. **P* < 0.05; ***P* < 0.01.

To functionally address the role of ERK as a potential downstream effector molecule for the EREG-induced promotion of tumor growth, we tested whether the ERK inhibitors U0126 and PD98059 could counteract EREG-mediated effects on IEC and tumors. Indeed, while EREG significantly enhanced the proliferation of colonic epithelial cells ($P < 0.01$), this effect was completely abrogated by ERK inhibitors (Figure 10B), suggesting that ERK signaling controls EREG-mediated effects on epithelial cell

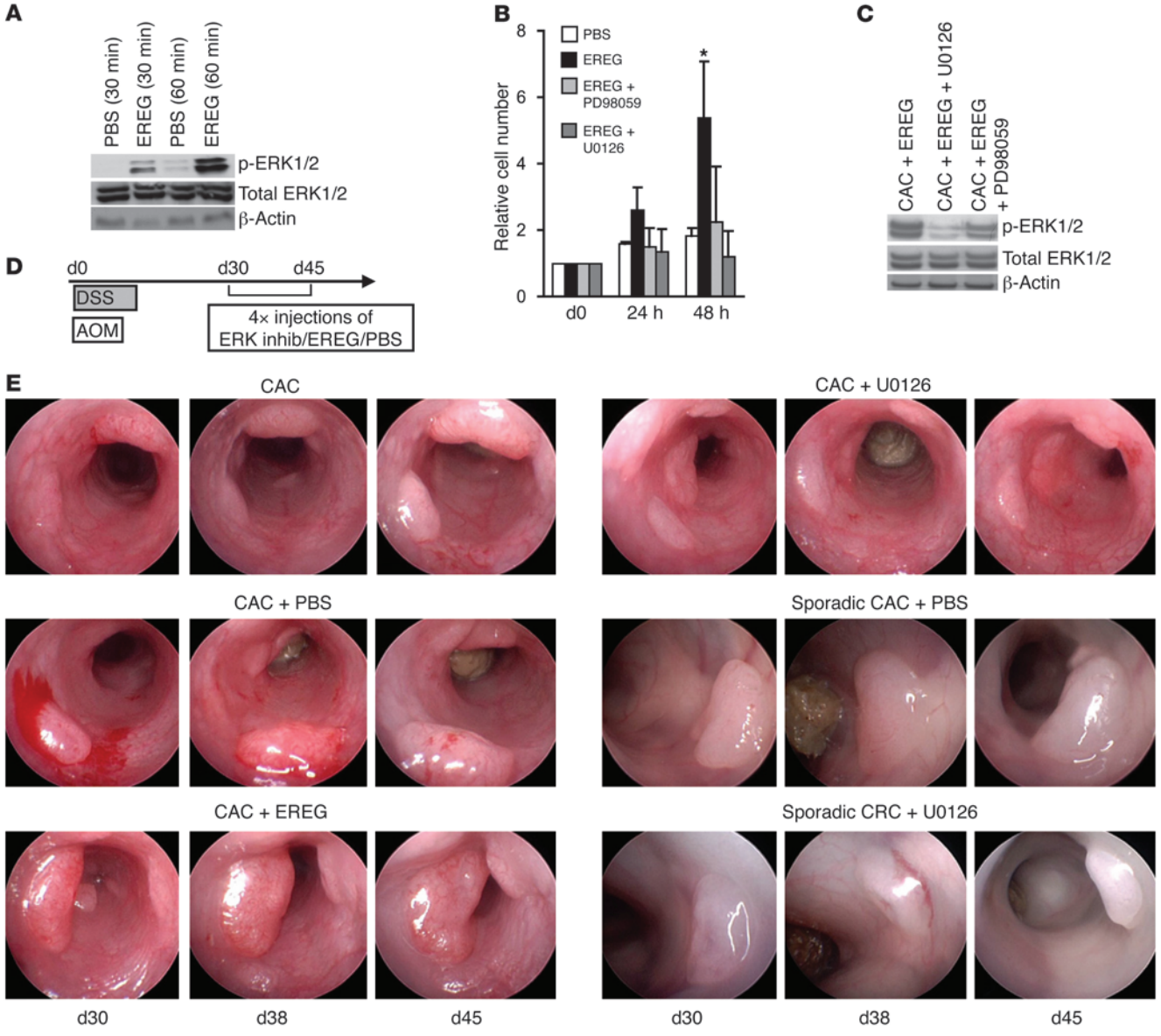

Figure 10

EREG promotes the development of colitis-associated tumors via activation of ERK. (**A**) CMT93 cells were cultured with EREG (100 ng/ml) or PBS. Cell lysates were quantified for phospho-ERK1/2, total ERK1/2, and β-actin by Western blots. (**B**) IEC were cultured in the presence of PBS or EREG (100 ng/ml) and ERK inhibitors PD98059 (1 μg/ml) or U0126 (40 ng/ml), as indicated. Cell numbers were determined after 24 and 48 hours. The experiment was performed twice with similar results. *$P < 0.05$. (**C**) Freshly harvested tumors of sizes 3–4 were cut into pieces and equally distributed into tissue culture wells. Next, tumor tissue was cultured with EREG and ERK inhibitors (U0126, PD98059). After 60 minutes, tumors were lysed and quantified for phospho-ERK1/2, total ERK1/2, and β-actin by Western blotting. The experiment was repeated twice with similar results. (**D**–**F**) Colitis-associated tumors were induced in WT mice by AOM and 1 cycle of DSS. *Apc*$^{min/+}$ mice were screened at the age of 6 weeks for the presence of sporadic rectosigmoidal tumors. Endoscopically guided injections of PBS, EREG, or ERK inhibitor (U0126) were made into growing tumors 4 times in 10 days starting at day 30. The change of tumor load was monitored by endoscopy until day 45. Data are from 1 out of 3 experiments and represent mean values ± SD (n = 3–5 per group). *$P < 0.05$.

proliferation. Furthermore, we detected that high levels of ERK phosphorylation in the AOM/DSS model could be blocked by incubation with these specific inhibitors despite the presence of EREG. These findings are consistent with ERK acting as the downstream effector of EREG-mediated tumor growth promotion in vitro and in vivo (Figure 10C). To address the in vivo relevance of this observation, we performed repetitive local injections into the base of small tumors during endoscopy and monitored tumor growth serially (Figure 10D). Interestingly, EREG injections resulted in accelerated tumor growth, while specific ERK inhibition with U0126 significantly suppressed tumor development (Figure 10, E and F). Of note, the same ERK inhibitor was markedly less potent in the *Apc*$^{min/+}$ model in sporadic colorectal tumorigenesis, as this inhibitor caused no significant reduction of tumor load in the *Apc*$^{min/+}$ model (Figure 10, E and F).

Thus, our data shows that interference with ERK signaling can block EREG-mediated growth promotion of experimental CAC.

Discussion

In the present study, we aimed to identify genes specifically involved in the development of CAC as opposed to sporadic CRC. By comparative gene expression analysis in murine models of CAC and CRC, we demonstrated that the protein EREG is specifically enriched in CAC and provided functional evidence that EREG functions as a key tumor growth promoter. Our findings are particularly remarkable considering that EREG-deficient mice develop more severe acute experimental colitis (16), excluding the possibility that EREG controls tumor growth by directly regulating colitis activity. Furthermore, we noted augmented expression of EREG in the colon of patients with IBD and colitis-associated dysplasia or CAC, highlighting the potential relevance of EREG for CAC growth in humans. In contrast, EREG expression in samples from sporadic tumor development was significantly lower and highly variable (24). To our knowledge, EREG is therefore the first epithelial growth factor to be recognized that preferentially controls growth of colitis-associated tumors.

In studies looking at the expression of EREG in the AOM/DSS model of colitis, we noted that EREG is repeatedly induced by flares in chronic colitis. In addition, tumor fibroblasts were identified as the major cellular source of EREG production in experimental colitis and patients with CAC. Functionally, EREG was shown to promote wound healing in IEC and experimental colitis in vivo by facilitating cell migration and activating proliferation of epithelial cells. Thus, our observations provide further evidence for a close association among intestinal injury, EREG induction, and EREG-mediated mucosal healing, which is consistent with recent work demonstrating high EREG production during intestinal injury (19, 25). In this context, it will be interesting to study a potential relationship between EREG and WNT5A in future studies, as WNT5A-dependent formation and subdivision of wound channels into crypts upon wounding has been very recently shown to be important during colonic crypt regeneration (26).

Several recent publications suggested that the inflammatory degree dictates the risk for colitis-associated tumor development (27, 28) Specifically, tumor development in the AOM/DSS model has been linked to STAT3 signaling in IEC induced by proinflammatory mediators such as IL-6 and IL-11 (29, 30). VEGF (31) and TNF receptor signaling events (32) also influence CAC growth in this model. Our findings highlight yet another key regulatory pathway mediated by EREG that drives tumor growth in experimental colitis. In contrast to the above mediators, however, EREG appears to specifically control inflammation-associated tumor growth in the AOM/DSS model rather than sporadic tumor growth in the *Apc*$^{min/+}$ model.

Tumor-associated fibroblasts were identified as key producers of EREG in experimental colitis–associated neoplasms and patients with CAC. The proinflammatory cytokine TNF-α was shown to be a potent inducer of EREG production, suggesting that TNF-α produced during experimental colitis (33) and human UC (34) drives EREG expression. Furthermore, the TLR4 ligand LPS markedly augmented EREG production. Of note, *Tlr4*$^{-/-}$ mice are more susceptible to experimental colitis, but are also protected from colitis-associated tumor development (35, 36). Another mechanism for EREG induction in colitis-associated neoplasms might involve hypomethylation, although we could not detect hypomethylation of the *Ereg* promoter (data not shown). Furthermore, EREG was a potent inducer of its own expression, suggesting the existence of autoregulatory loops augmenting EREG levels.

The role of cancer-associated fibroblasts in tumorigenesis has not been fully clarified yet. However, previous studies reported that such fibroblasts include subpopulations that are highly heterogeneous (37, 38). Furthermore, it was found that these cells have pleiotropic functions and may favor tumor promotion via secreted growth and angiogenic factors such as IL-8 (39), VEGF (31, 40), FGF-2 (41), and SDF-1 (42). Additional publications have highlighted a crucial role of cancer-associated fibroblasts in inflammation-associated carcinogenesis of the skin and stomach, respectively (43, 44). In contrast, the role of these cells in colitis-associated tumorigenesis has not been previously addressed. Here, we demonstrated that EREG is expressed by tumor-associated fibroblasts in the AOM/DSS model and patients with colitis-associated neoplasms. As the acquisition of a myofibroblastic phenotype is a common feature for tumor-associated fibroblasts (45), we analyzed the relationship between α-SMA–expressing fibroblasts and EREG expression in the AOM/DSS model. It was found that EREG expression is not limited to α-SMA–expressing tumor-associated fibroblasts, which is in line with studies showing that the tumor-promoting properties of tumor-associated fibroblasts are not mandatorily linked to α-SMA expression (37, 43). Subsequently, we took advantage of a newly developed adoptive transfer system to demonstrate that EREG producing, but not EREG-deficient, tumor-associated fibroblasts augment tumor cell growth in experimental colitis–associated neoplasms. These findings underline what we believe is a novel role of tumor-associated fibroblasts in colitis-associated neoplasms by directly stimulating cell proliferation via EREG production.

EREG has previously been shown to induce EGFR phosphorylation and cell proliferation in IEC (19, 23), and such EGFR signaling is known to induce ERK activation (27, 46, 47). Studies on the signaling events induced by EREG activation showed induction of ERK upon stimulation of IEC with EREG. Functional studies using ERK blockade revealed that ERK is essential for EREG-mediated induction of epithelial cell proliferation, suggesting that ERK and EGFR induce tumor cell growth. However, we cannot rule out that other ERBB family receptors may be involved in EREG signaling, since EREG can also signal via other ERBB molecules (48). Furthermore, selective targeting of EGFR signaling has been recently suggested to augment tumor growth in the AOM/DSS model (27), consistent with the idea that other ERBB receptors might be involved in EREG signaling. Nevertheless, ERK inhibi-

tors suppressed the proliferative effects of EREG on epithelial cells in the AOM/DSS model in vivo, highlighting a crucial role of ERK for EREG function. Interestingly, ERK activation has recently been reported to drive sporadic intestinal tumorigenesis in *Apc*$^{min/+}$ mice (49), and EGFR blockade resulting in ERK inhibition has been successfully applied in *Apc*$^{min/+}$ mice in the intestine (50). However, our study indicates that ERK inhibition is substantially more potent in the AOM/DSS model of CAC, suggesting that ERK blockade might be particularly effective as a novel therapeutic strategy for patients with CAC.

The EREG/ERK pathway appears to be particularly relevant for inflammation-associated colorectal tumors, as mucosal inflammation results in marked production of potent EREG inducers such as LPS and TNF-α. Subsequently, EREG may further augment its own production by an autoregulatory feedback loop in tumor-associated fibroblasts, thereby explaining the particular relevance of EREG for inflammation-associated neoplasms. Thus, our data suggest that ERK activation links EREG to the growth of CAC. The functional relevance of these findings was underlined by the observation that growth of experimental CAC could be induced by transfer of EREG-producing tumor-associated fibroblasts or recombinant EREG via ERK activation, while EREG deficiency substantially suppressed tumor growth. Thus, inhibition of EREG function and blockade of EREG production by tumor-associated fibroblasts emerges as a promising innovative approach for the blockade of colitis-associated tumorigenesis. As patients with CAC show markedly higher levels of EREG than controls, these results open new avenues for therapy of this disease.

Methods

Mice. *Ereg*$^{-/-}$ mice (B6.129S6-*Ereg*^{tm1Dwt}) are genetically altered by a β-geo cassette knocked into the first exon of the *Ereg* gene, as previously described (16). Our studies included animals from P.-L. Tharaux′ colony of *Ereg*$^{-/-}$ mice (Laboratory for Optics and Biosciences & Cardiovascular Research Center, Inserm Ecole Polytechnique, Paris, France). *Ereg*$^{-/-}$ mice had been bred congenic onto C57BL/J for more than 10 generations. C57BL/6J-*Apc*$^{min/+}$/J and control mice on the same genetic background were obtained from the animal facilities of the Johannes Gutenberg-Universität Mainz and the Medical Clinic 1, Friedrich-Alexander-Universität Erlangen-Nürnberg. All mice were kept under specific pathogen–free conditions.

Human samples. Human specimens were obtained from the Institute of Pathology in Bayreuth and the Medical Clinic 1, Friedrich-Alexander-Universität Erlangen-Nürnberg, where they had been taken from routine colonoscopic samples. The analysis included 47 samples (non-IBD control patients, n = 7; sporadic HGD, n = 12, sporadic CRC, n = 11; colitis-associated HGD, n = 9; CAC, n = 8).

Experimental models and tumor growth observation. For investigations into experimental colitis–associated tumorigenesis, a single i.p. injection of AOM (10 mg/kg) (Sigma-Aldrich) was followed by 3 cycles of DSS administration, with each cycle comprising 1 week of 2.5% (w/v) DSS (MP Biomedicals) in drinking water followed by 2 weeks of regular water (14). For studies of sporadic tumorigenesis, the *Apc*$^{min/+}$ model was used (12). Tumor development was monitored by the Colorview endoscopic system (Karl Storz), as previously described (15). Chronically relapsing colitis was induced by 3 cycles of 2.5% DSS, as described above.

Tissue harvest and purification. Tumors were harvested at size 4 in endoscopic scoring (15). All tumors and control epithelia that were included in HDMA originated from the lower sixth of the colon. Epithelial purification was performed as previously described (51) with slight modifications. In brief, distal colonic specimens were incubated in prewarmed HBSS supplemented with EDTA (2 mM), EGTA (1 mM), DTT, and FCS (1%) with gentle agitation at 37°C for 20 minutes. The epithelial purity was routinely at 80%–85%, as assessed by microscopic quantitative analysis.

For RNA purification, tumors and purified distal colon epithelium were placed in RNeasy lysis buffer (QIAGEN), disrupted, and homogenized using a master mill before being processed by using RNeasy Mini Kits (QIAGEN).

High-density microarray analysis. Whole-genome transcriptome analysis was performed with 5 μg high quality total RNA per sample at the HDMA core facility of the Johannes Gutenberg-Universität in Mainz. Data analysis was performed with ArrayAssist and PathwayArchitect software (Agilent Technologies). Details about microarray analysis have been deposited under accession number GSE43338 at NCBI GEO.

Multispectral fluorescence imaging. Multispectral fluorescence imaging was done with the Maestro imaging system (Intas). Integrin $\alpha_v\beta_3$ expression could be visualized after i.v. injection of 100 μl fluorescence dye integriSense (Visen Medical).

Histopathological and immunohistochemical stainings. Histopathological analysis was performed on paraffin-embedded tissue after H&E staining. Immunofluorescence of cryosections or paraffin-embedded tissue was done using the TSA Cy3 system (PerkinElmer) (17). Primary antibodies were goat anti-human EREG (polyclonal; R&D), rabbit anti-human FSP1/S100A4 (polyclonal; Lifespan Bioscience), rabbit anti-human PDGFR-β (clone 28E1; Cell Signaling), rabbit anti-mouse α-SMA (polyclonal, Abcam), and rat anti-mouse Ki67 (Dako). Rabbit anti-human VIM was used as an AF488-conjugated antibody (Cell Signaling). Nuclei were counterstained with DAPI (Invitrogen), and fluorescence analysis was performed with an IX70 (Olympus) or SP5 (Leica). LacZ staining on tumors or purified cells was performed as previously described (16). For quantitative analyses, 4–5 representative high power fields (×40) per sample were scored in a blinded fashion.

Fibroblast purification. For fibroblast isolation, colonic tumors were cut into small pieces and incubated with complete medium including antibiotics and antimycotics for 15 minutes at 37°C. After 2 washes, tumor pieces were incubated with an enzyme cocktail made of trypsin (2.5 mg/ml; Difco), collagenase IV (400 U/ml), and DNase1 (350 U/ml) for 30 minutes at 37°C. The supernatant containing the cell suspension was removed and filled with complete medium. The remaining tissue was incubated with enzyme cocktail for another 30 minutes at 37°C. If necessary, the tissue was further disintegrated by passing through a 23-gauge needle. Next, all cell suspensions were combined and filtered through a 100-μm cell strainer. After additional washes, cells were cultured in tissue culture flasks and medium was renewed after 1 day and subsequently when necessary. Adhering fibroblasts grew to confluence within some days.

Protein isolation and Western blotting. Proteins were purified from intestinal specimens with the M-PER mammalian protein extraction reagent according to the manufacturer's recommendations (Pierce Biotechnology). Western blotting was performed using the ECL Analysis System (GE Healthcare), as previously described (17). Antibodies were from Cell Signaling Technology (anti-p44/42-MAPK, anti phospho-p44/42-MAPK) or Santa Cruz Biotechnology Inc. (anti-ACTB).

Wound healing. For intestinal wound-healing studies in vivo, mucosal lesions of 800 μm in diameter were generated with a biopsy forceps during mini-endoscopy (20). The wound-healing process was followed by endoscopic evaluations every 1–2 days until the lesion had been resolved.

For the analysis of cell migration in vitro, murine IEC (CMT93) were grown to confluence in serum-free medium. Then, standardized gaps of approximately 650 μm in diameter were scratched into the cell layer using a pipette tip, and the cell-culture system was supplemented as specified. The process of wound gap closure was monitored and quantified by microscopy (IX70; Olympus).

In vitro and ex vivo colon cell and tumor studies. For in vitro proliferation studies, murine IEC (CMT93) were seeded at almost confluence using equal numbers and grown in the presence of various concentrations of recombinant EREG (R&D) or ERK-inhibitors PD98059 (Merck) or U0126 (Merck) and cell numbers were counted at different time points. For in vitro stimulation experiments, TNF-α and IL-6 were purchased from Immunotools; LPS and lipoteichoic acid (LTA) were from Invivogen.

For ex vivo tumor studies, freshly harvested tumors were cut into pieces and equally distributed over tissue culture wells, where they were cultured, as specified (Figure 10), i.e., in the presence of EREG and /or different ERK inhibitors.

Fibroblast transfer studies. For fibroblast transfer studies, tumors were induced in *Ereg*$^{-/-}$ or WT mice by AOM (10 mg/kg) and 1 cycle of DSS (2.5%). At day 30, all animals were endoscopically screened, and then mice with early tumors were equally assigned to the experimental groups. Starting at day 30, local injections were performed as previously described (20, 32). In detail, fibroblasts were injected into growing tumors via a mini-injection needle introduced through the working channel of the endoscope. The fibroblast transfer was performed with 10^5 cells per injection at volumes of 50 μl, and 4 applications were done within 15 days. The change of tumor load was monitored by endoscopy.

For other in vivo studies, EREG (200 ng, R&D), EGF (200 ng, Immunotools), AREG (200 ng, R&D), or U0126 (20 ng, Merck) was locally injected 4 times in 10 days at volumes of 50 μl.

Statistics. Significance analysis of normally distributed data was performed using 1-tailed Student's *t* test. Error bars represent SD. To reduce the false discovery rate in microarray data, *P* value correction by Benjamini-Hochberg was applied. *P* values of less than 0.05 and 0.01 were considered significant and highly significant, respectively.

Study approval. Animal studies were performed in accordance with German law and with approval from Landesuntersuchungsamt Rheinland-Pfalz, (Koblenz, Germany) and Regierung Mittelfranken (Ansbach, Germany). The collection of human intestinal biopsies was approved by Ethik-Kommission der Medizinischen Fakultät der Friedrich-Alexander-Universität, Erlangen-Nürnberg. All subjects provided informed consent prior to their participation in the study.

Acknowledgments

We thank P.-L. Tharaux (Paris, France) for sending *Ereg*$^{-/-}$ animals from his colony. The authors appreciate helpful discussions with U. Luxemburger and M. Kozlowski (Mainz, Germany) regarding microarray analysis. We thank A. Nikolaev (Mainz, Germany), I.-Zöller-Utz, D. Fröba, and S. Wallmüller (Erlangen, Germany) for excellent technical assistance. This study was supported by grants from United European Gastroenterology (to C. Neufert, top abstract prize 2011; M.F. Neurath, research prize 2008), by ELAN-Fonds and IZKF-Fonds of Friedrich-Alexander-Universität Erlangen-Nürnberg (to C. Neufert), and by the DFG (GK1043/2, KFO257 to C. Becker and M.F. Neurath).

Received for publication November 26, 2012, and accepted in revised form January 24, 2013.

Address correspondence to: Markus F. Neurath, Medical Clinic 1, Friedrich-Alexander University Erlangen-Nürnberg, Ulmenweg 18, D-91054 Erlangen, Germany. Phone: 09131.85.35000; Fax: 09131.85.35209; E-mail: markus.neurath@uk-erlangen.de.

1. Danese S, Fiocchi C. Ulcerative colitis. *N Engl J Med*. 2011;365(18):1713–1725.
2. MacDonald TT, Monteleone I, Fantini MC, Monteleone G. Regulation of homeostasis and inflammation in the intestine. *Gastroenterology*. 2011; 140(6):1768–1775.
3. Strober W, Fuss I, Mannon P. The fundamental basis of inflammatory bowel disease. *J Clin Invest*. 2007; 117(3):514–521.
4. Ekbom A, Helmick C, Zack M, Adami HO. Ulcerative colitis and colorectal cancer. A population-based study. *N Engl J Med*. 1990;323(18):1228–1233.
5. Jess T, et al. Risk of intestinal cancer in inflammatory bowel disease: a population-based study from olmsted county, Minnesota. *Gastroenterology*. 2006;130(4):1039–1046.
6. Ullman TA, Itzkowitz SH. Intestinal inflammation and cancer. *Gastroenterology*. 2011;140(6):1807–1816.
7. Meira LB, et al. DNA damage induced by chronic inflammation contributes to colon carcinogenesis in mice. *J Clin Invest*. 2008;118(7):2516–2525.
8. Leclerc D, Deng L, Trasler J, Rozen R. ApcMin/+ mouse model of colon cancer: gene expression profiling in tumors. *J Cell Biochem*. 2004;93(6):1242–1254.
9. Terzic J, Grivennikov S, Karin E, Karin M. Inflammation and colon cancer. *Gastroenterology*. 2010; 138(6):2101–2114.e5.
10. Rakoff-Nahoum S, Medzhitov R. Regulation of spontaneous intestinal tumorigenesis through the adaptor protein MyD88. *Science*. 2007; 317(5834):124–127.
11. Uronis JM, Muhlbauer M, Herfarth HH, Rubinas TC, Jones GS, Jobin C. Modulation of the intestinal microbiota alters colitis-associated colorectal cancer susceptibility. *PLoS One*. 2009;4(6):e6026.
12. Moser AR, Pitot HC, Dove WF. A dominant mutation that predisposes to multiple intestinal neoplasia in the mouse. *Science*. 1990;247(4940):322–324.
13. Tanaka T, Kohno H, Suzuki R, Yamada Y, Sugie S, Mori H. A novel inflammation-related mouse colon carcinogenesis model induced by azoxymethane and dextran sodium sulfate. *Cancer Sci*. 2003; 94(11):965–973.
14. Neufert C, Becker C, Neurath MF. An inducible mouse model of colon carcinogenesis for the analysis of sporadic and inflammation-driven tumor progression. *Nat Protoc*. 2007;2(8):1998–2004.
15. Becker C, et al. In vivo imaging of colitis and colon cancer development in mice using high resolution chromoendoscopy. *Gut*. 2005;54(7):950–954.
16. Lee D, Pearsall RS, Das S, Dey SK, Godfrey VL, Threadgill DW. Epiregulin is not essential for development of intestinal tumors but is required for protection from intestinal damage. *Mol Cell Biol*. 2004;24(20):8907–8916.
17. Becker C, et al. TGF-beta suppresses tumor progression in colon cancer by inhibition of IL-6 transsignaling. *Immunity*. 2004;21(4):491–501.
18. Greten FR, et al. IKKbeta links inflammation and tumorigenesis in a mouse model of colitis-associated cancer. *Cell*. 2004;118(3):285–296.
19. Hsu D, et al. Toll-like receptor 4 differentially regulates epidermal growth factor-related growth factors in response to intestinal mucosal injury. *Lab Invest*. 2010;90(9):1295–1305.
20. Neurath MF, et al. Assessment of tumor development and wound healing using endoscopic techniques in mice. *Gastroenterology*. 2010;139(6):1837–1843.
21. Tlsty TD, Coussens LM. Tumor stroma and regulation of cancer development. *Annu Rev Pathol*. 2006; 1:119–150.
22. Abraham C, Medzhitov R. Interactions between the host innate immune system and microbes in inflammatory bowel disease. *Gastroenterology*. 2011; 140(6):1729–1737.
23. Oda K, Matsuoka Y, Funahashi A, Kitano H. A comprehensive pathway map of epidermal growth factor receptor signaling. *Mol Syst Biol*. 2005; 1:2005.0010.
24. Khambata-Ford S, et al. Expression of epiregulin and amphiregulin and K-ras mutation status predict disease control in metastatic colorectal cancer patients treated with cetuximab. *J Clin Oncol*. 2007; 25(22):3230–3237.
25. Brandl K, et al. MyD88 signaling in nonhematopoietic cells protects mice against induced colitis by regulating specific EGF receptor ligands. *Proc Natl Acad Sci U S A*. 2010;107(46):19967–19972.
26. Miyoshi H, Ajima R, Luo CT, Yamaguchi TP, Stappenbeck TS. Wnt5a potentiates TGF-beta signaling to promote colonic crypt regeneration after tissue injury. *Science*. 2012;338(6103):108–113.
27. Dube PE, et al. Epidermal growth factor receptor inhibits colitis-associated cancer in mice. *J Clin Invest*. 2012;122(8):2780–2792.
28. Dupaul-Chicoine J, et al. Control of intestinal homeostasis, colitis, and colitis-associated colorectal cancer by the inflammatory caspases. *Immunity*. 2010;32(3):367–378.
29. Bollrath J, et al. gp130-mediated Stat3 activation in enterocytes regulates cell survival and cell-cycle progression during colitis-associated tumorigenesis. *Cancer Cell*. 2009;15(2):91–102.
30. Grivennikov S, et al. IL-6 and Stat3 are required for survival of intestinal epithelial cells and development of colitis-associated cancer. *Cancer Cell*. 2009; 15(2):103–113.
31. Waldner MJ, et al. VEGF receptor signaling links inflammation and tumorigenesis in colitis-associated cancer. *J Exp Med*. 2010;207(13):2855–2868.
32. Popivanova BK, et al. Blocking TNF-alpha in mice reduces colorectal carcinogenesis associated with chronic colitis. *J Clin Invest*. 2008;118(2):560–570.
33. Neurath MF, et al. Predominant pathogenic role of tumor necrosis factor in experimental colitis in mice. *Eur J Immunol*. 1997;27(7):1743–1750.
34. Breese EJ, et al. Tumor necrosis factor alpha-producing cells in the intestinal mucosa of children with inflammatory bowel disease. *Gastroenterology*. 1994; 106(6):1455–1466.
35. Fukata M, et al. Toll-like receptor-4 is required for intestinal response to epithelial injury and limiting bacterial translocation in a murine model of acute

colitis. *Am J Physiol Gastrointest Liver Physiol*. 2005; 288(5):G1055–G1065.
36. Fukata M, et al. Toll-like receptor-4 promotes the development of colitis-associated colorectal tumors. *Gastroenterology*. 2007;133(6):1869–1881.
37. Sugimoto H, Mundel TM, Kieran MW, Kalluri R. Identification of fibroblast heterogeneity in the tumor microenvironment. *Cancer Biol Ther*. 2006; 5(12):1640–1646.
38. Franco OE, Shaw AK, Strand DW, Hayward SW. Cancer associated fibroblasts in cancer pathogenesis. *Semin Cell Dev Biol*. 2010;21(1):33–39.
39. Anderson IC, Mari SE, Broderick RJ, Mari BP, Shipp MA. The angiogenic factor interleukin 8 is induced in non-small cell lung cancer/pulmonary fibroblast cocultures. *Cancer Res*. 2000;60(2):269–272.
40. Bergers G, et al. Matrix metalloproteinase-9 triggers the angiogenic switch during carcinogenesis. *Nat Cell Biol*. 2000;2(10):737–744.
41. Nissen LJ, et al. Angiogenic factors FGF2 and PDGF-BB synergistically promote murine tumor neovascularization and metastasis. *J Clin Invest*. 2007; 117(10):2766–2777.
42. Orimo A, et al. Stromal fibroblasts present in invasive human breast carcinomas promote tumor growth and angiogenesis through elevated SDF-1/CXCL12 secretion. *Cell*. 2005;121(3):335–348.
43. Erez N, Truitt M, Olson P, Arron ST, Hanahan D. Cancer-associated fibroblasts are activated in incipient neoplasia to orchestrate tumor-promoting inflammation in an NF-kappaB-dependent manner. *Cancer Cell*. 2010;17(2):135–147.
44. Quante M, et al. Bone marrow-derived myofibroblasts contribute to the mesenchymal stem cell niche and promote tumor growth. *Cancer Cell*. 2011; 19(2):257–272.
45. Kalluri R, Zeisberg M. Fibroblasts in cancer. *Nat Rev Cancer*. 2006;6(5):392–401.
46. Egger B, Buchler MW, Lakshmanan J, Moore P, Eysselein VE. Mice harboring a defective epidermal growth factor receptor (waved-2) have an increased susceptibility to acute dextran sulfate-induced colitis. *Scand J Gastroenterol*. 2000;35(11):1181–1187.
47. Roberts RB, et al. Importance of epidermal growth factor receptor signaling in establishment of adenomas and maintenance of carcinomas during intestinal tumorigenesis. *Proc Natl Acad Sci U S A*. 2002; 99(3):1521–1526.
48. Shelly M, et al. Epiregulin is a potent pan-ErbB ligand that preferentially activates heterodimeric receptor complexes. *J Biol Chem*. 1998; 273(17):10496–10505.
49. Lee SH, et al. ERK activation drives intestinal tumorigenesis in Apc(min/+) mice. *Nat Med*. 2010; 16(6):665–670.
50. Shaw PH, Maughan TS, Clarke AR. Dual inhibition of epidermal growth factor and insulin-like 1 growth factor receptors reduce intestinal adenoma burden in the Apc(min/+) mouse. *Br J Cancer*. 2011; 105(5):649–657.
51. Nenci A, et al. Epithelial NEMO links innate immunity to chronic intestinal inflammation. *Nature*. 2007;446(7135):557–561.